Palaeogeography, Palaeoclimatology, Palaeoecology 514 (2019) 441–452

Contents lists available at ScienceDirect

Palaeogeography, Palaeoclimatology, Palaeoecology

journal homepage: www.elsevier.com/locate/palaeo

Vegetation and climate evolution during the Last Glaciation at Tengchong in Yunnan Province, Southwest China

Jixiao Zhang[a,c,d], Hai Xu[b,*], William D. Gosling[d], Jianghu Lan[a], John Dodson[a], Fengyan Lu[a], Keke Yu[a], Enguo Sheng[a], Bin Liu[a]

[a] Institute of Earth Environment, Chinese Academy of Sciences, 710061 Xi'an, China
[b] Institute of Surface-Earth System Science, Tianjin University, 300072 Tianjin, China
[c] University of Chinese Academy of Sciences, 100049 Beijing, China
[d] Paleoecology & Landscape Ecology, Institute for Biodiversity & Ecosystem Dynamics (IBED), University of Amsterdam, 1090 GE Amsterdam, the Netherlands

ARTICLE INFO

Keywords:
Peatland
Microfossil
Pollen
Principal component analysis
Geochemistry
Heinrich events

ABSTRACT

To better understand changes in vegetation and climate during the Last Glaciation in Southwest (SW) China, we studied microfossil assemblages in a peat/lake-sediment core collected in Tengchong Basin that spans the interval 66.6–11.8 ka (1 ka = 1000 cal yr BP), approximately equivalent to marine isotope stages (MIS) 4 to 2. The results show that patterns of climate change in Tengchong during the Last Glaciation were different from those in eastern China, and suggest that, compared with modern climates, SW China was cool and semi-humid during MIS 4, cold and semi-humid in the early and middle stages of MIS 3, and cool and humid in the late stage of MIS 3. During the Last Glacial Maximum (LGM), it was cool and dry, whereas after the LGM the climate remained dry but became warmer. Down-core changes in *Abies* and *Picea* pollen amongst the woody plants broadly match records of geochemical indices in parallel peat/lake-sediment cores and stalagmite oxygen isotope records from monsoonal Asia. Heinrich events 1–5 and volcanic eruption events are recognized in the *Abies* + *Picea* curve. As inferred from the microfossil assemblages in the Tengchong cores, the coldest interval in SW China during the Last Glaciation might not have been the LGM.

1. Introduction

The Last Glaciation spans the interval ca. 110.0–11.7 ka (Ehlers et al., 2004), the global temperatures during the Last Glaciation are inferred to have been lower than present, as shown by relatively high marine $\delta^{18}O$ values in marine isotope stages (MIS) 4–2 (Ono and Naruse, 1997; Helmens, 2014). Previous studies suggest that climatic changes in China during the Last Glaciation are generally consistent with the global signal (Porter and An, 1995). However, because of the complex geography of China, it is likely that climate change in China had different manifestations in different regions (Fu et al., 2008).

Southwest (SW) China, including Yunnan Province, Guizhou Province, Sichuan Province, Chongqing Municipality, and the Tibet Autonomous Region, is located in the transition zone between the Indian Summer Monsoon (ISM) and the East Asian Summer monsoon (Ha et al., 2017; Wang et al., 2001), and lies near the tropical/subtropical boundary. Generally, the climate is mild. Previous studies on the Last Glaciation have suggested that patterns of climate change in SW China were more influenced by the ISM and differed from those in eastern China (Tian and Jiang, 2016). For example, it has been suggested that during MIS 3, SW China was cooler and wetter than modern times, while southeast (SE) China was warmer (Zhen et al., 2008). However, these conclusions are based on limited evidence and need to be further investigated (Huang et al., 2003).

Tengchong County in Yunnan Province is an area affected by the ISM, according to precipitation data (Zhu et al., 2017), thus making it a suitable study area to investigate paleoclimatic change related to the ISM. Qinghai is a crater lake located in Tengchong that contains a relatively long depositional sequence. Several paleoclimate and paleovegetation studies have been carried out around this area (Zhang et al., 2015; Long et al., 2015; Xiao et al., 2016, 2017; Yang et al., 2016), but with a focus mainly on the Last Glacial Maximum (LGM) and Holocene, and lack data from earlier periods. Although longer-scale paleoclimatic records do exist from nearby areas, the temporal resolution of these records is poor, thus hindering further comparisons between pollen data and other indices (Zhang et al., 2004; Hu et al., 2005, 2015; Xiao et al., 2014). To solve these problems, we present new relatively high resolution microfossil data from Tengchong to shed light on regional

* Corresponding author.
E-mail address: xuhai@tju.edu.cn (H. Xu).

https://doi.org/10.1016/j.palaeo.2018.11.008
Received 1 April 2018; Received in revised form 31 October 2018; Accepted 1 November 2018
Available online 09 November 2018
0031-0182/

climate differences.

During the Last Glaciation, a large number of peat and lake sediments were deposited in SW China (Zhao et al., 2014). Down-core records of geochemical indices from Tengchong have been generated, and inferred climate change have been broadly discussed (Xu et al., 2016). Here we use an approach including analysis of pollen, spores, and other microfossils, to provide an understanding of paleovegetation and paleoclimate in SW China. These data are used to discuss the vegetation and climate changes during the Last Glaciation in SW China, and the results are then compared with published information on changes in geochemical indices and climate in adjacent areas to explore the causes of those changes.

2. Study area

Tengchong County is located in the southwest of Yunnan Province, at the southern end of the Hengduan Mountains, west of Gaoligong Mt. (Wang et al., 2007). The central area of Tengchong is relatively low in elevation, thus allowing the formation of lakes and peatlands. Tengchong has a northern subtropical climate, characterized by a) a small annual temperature difference, b) a mean annual temperature of 14–16 °C, c) temperatures during the coldest month of 7.5–10 °C, d) temperatures during the hottest month of 19–21 °C, and d) mean annual precipitation of 1000–1500 mm. Previous studies have shown that precipitation in this region increases linearly with altitude, with gradients between 20 mm/100 m and 85 mm/100 m; thus, high altitudes are more humid than lower altitudes (Wu and Li, 2004).

The natural vegetation at Tengchong today is characterized by northern subtropical evergreen broad-leaved forest (Fig. 1) that varies over an altitude gradient (Wu et al., 1987), as follows.

i) Below 1500 m asl (above sea level) hot–dry valley savanna is the dominant vegetation type, with abundant Poaceae-based grasslands.
ii) Between 1500 and 2500 m asl, the typical vegetation type is evergreen broad-leaved forest and *Pinus* forest, with common species including *Castanopsis*, *Cyclobalanopsis*, and *Lithocarpus*, and abundant ferns beneath the forest canopy.
iii) Areas between 2500 and 2800 m asl are dominated by *Lithocarpus* evergreen broad-leaved forest.
iv) From 2800 to 3200 m asl, *Tsuga* forest or *Tsuga*–evergreen–deciduous broad-leaved mixed forest is dominant.
v) Areas between 3200 and 4200 m asl are dominated by *Abies*- and *Picea*-based cold temperate coniferous forest, also referred to as boreal forest. Alpine Ericaceae shrub and meadows are distributed around 4000 m asl.

Peatland areas are distributed mainly between 1600 and 1700 m asl, and populations of aquatic plants vary across the region (Shen and Liang, 2005).

3. Material, methods, and chronology

The material and chronology used in this study is consistent with Xu et al. (2016). The study site is located in the Tengchong Basin (25°00′37″N, 98°31′26″E, 1630 m asl), and is now a paddy field. Three sediment cores were recovered from the same site: TC-11-1 (December 2011), TC-14-1, and TC-14-2 (April 2014). These cores are almost parallel, but differ slightly in length and are incomplete. As a result, they were aligned using density data and high-resolution magnetic susceptibility readings to generate the most complete sedimentary sequence possible. The intervals 0–220 cm, 221–620 cm, 621–672 cm come from TC-11-1, TC-14-2, and TC-14-2, respectively. After the alignment, a composite sedimentary sequence was established for the Tengchong site. According to changes in lithology, the sedimentary sequence can be divided into four parts: i) the top 0–46 cm is a modern till age layer, which was not used for analysis; ii) the interval 47–270 cm is composed of peat; iii) 271–570 cm consists of lacustrine sediments; and iv) the interval 571–672 cm is another peat layer. Plant residues and/or cellulose extracted from peat deposits (46–270 cm) were selected for ^{14}C dating, and the results were calibrated with Calib 6.02 software, giving ages spanning 11.8 to 28 ka. The underlying lacustrine/peat layers (271–672 cm) were dated via OSL dating, and yielded ages spanning 28–70 ka. The age model is supported by tephra and correlates well with the Asian speleothem $\delta^{18}O$ curve.

One hundred samples were selected from the composite Tengchong sedimentary sequence for fossil pollen analysis. Fossil pollen was extracted using standard procedures, including the application of hydrofluoric acid (Bates et al., 1978). An exotic *Lycopodium* spore tablet (University of Lund, batch 483,216, containing 18,583 ± 764 *Lycopodium* per tablet) was added to each sample to calculate pollen concentrations (Stockmarr, 1971). Pollen and other microfossils were identified and counted at ×400 and ×1000 magnification using a light microscope (Olympus BX53), referring to the modern pollen slides from Yunnan Province and references (Zhang, 1990; Wang, 1995). At least 200 pollen and spore grains were counted for each sample, which is adequate to assess changes in the percentage of dominant types (Brush and DeFries, 1981; Madanes and Dadon, 1998; Pearsall, 2015; Kou et al., 2006). The microfossil diagram and DCA/PCA plots were drawn using Tilia 1.7.16 (Grimm, 2011) and Canoco 4.5 (ter Braak and Smilauer, 2002), respectively.

4. Results

4.1. Types of pollen, spores, and algae

A total of 57 main types of pollen, spores, and algae (hereafter microfossils; Fig. 2) are identified in the samples (taxa that are only present in one sample and that make up < 0.5% of the assemblage are not included in these statistics). These include 27 types of woody taxa (*Pinus*, *Abies*, *Picea*, *Tsuga*, *Quercus*, *Cyclobalanopsis*, *Lithocarpus/Castanopsis*, *Alnus*, *Betula*, *Juglans*, *Carya*, *Pterocarya*, Rutacaeae, Oleaceae, *Bignonia*, Sapindaceae, *Ulmus*, Ericaceae, *Liquidambar*, *Tilia*, Moraceae, Elaeagnaceae, *Ilex*, Myrtaceae, *Hibiscus*, Piperaceae, *Symplocos*); 26 types of herbaceous taxa (Cyperaceae, Poaceae, Euphorbiaceae, *Aster*-type, *Taraxacum*-type, *Artemisia*-type, *Polygonum*, *Geranium*, *Gentiana*, *Hygrophila*, Ranunculaceae, Caryophyllaceae, Liliaceae, Brassicaceae, Rubiaceae, Fabaceae, *Chenopodium*, Onagraceae, Verbenaceae, Apiaceae, Solanaceae, Araceae, *Potentilla*, Balsaminaceae, *Commelina*, Cucurbitaceae); 2 types of fern spore (Trilete spores and Monolete spores); and 2 types of algae (*Spirogyra* and *Mougeotia*). The main species identified in the samples are similar to previous studies at Tengchong (Xiao et al., 2016; Yang et al., 2016).

4.2. Microfossil diagram and descriptions of assemblage zones

The microfossil diagram and cluster analyses are based on changes in the percentage of pollen, spores, and algae relative to total microfossils. Six main zones can be recognized from the Tengchong Core according to the microfossil assemblages and cluster analysis (Fig. 3). The zone boundaries are consistent with the divisions of the last glacial stage in China (Zhao et al., 2011a). The features of the microfossil assemblages in each zone are described below.

In Zone I (672–585 cm; 66.0–58.5 ka), the microfossil concentrations are relatively high, with an average of 11,267 grains/g. This zone is characterized by assemblages of Monolete spores–Poaceae–*Pinus*–*Tsuga*. Trees and shrubs account for 54.2% of the assemblage on average, while herbs account for 23.4%, fern spores for 22.4%, and algae for < 0.1%.

In Zone II-a (584–370 cm; 58.5–44.9 ka), microfossil concentrations are lower, with an average of 3533 grains/g. This zone is characterized by assemblages of Monolete spores–*Tsuga*–*Pinus*. Trees and shrubs

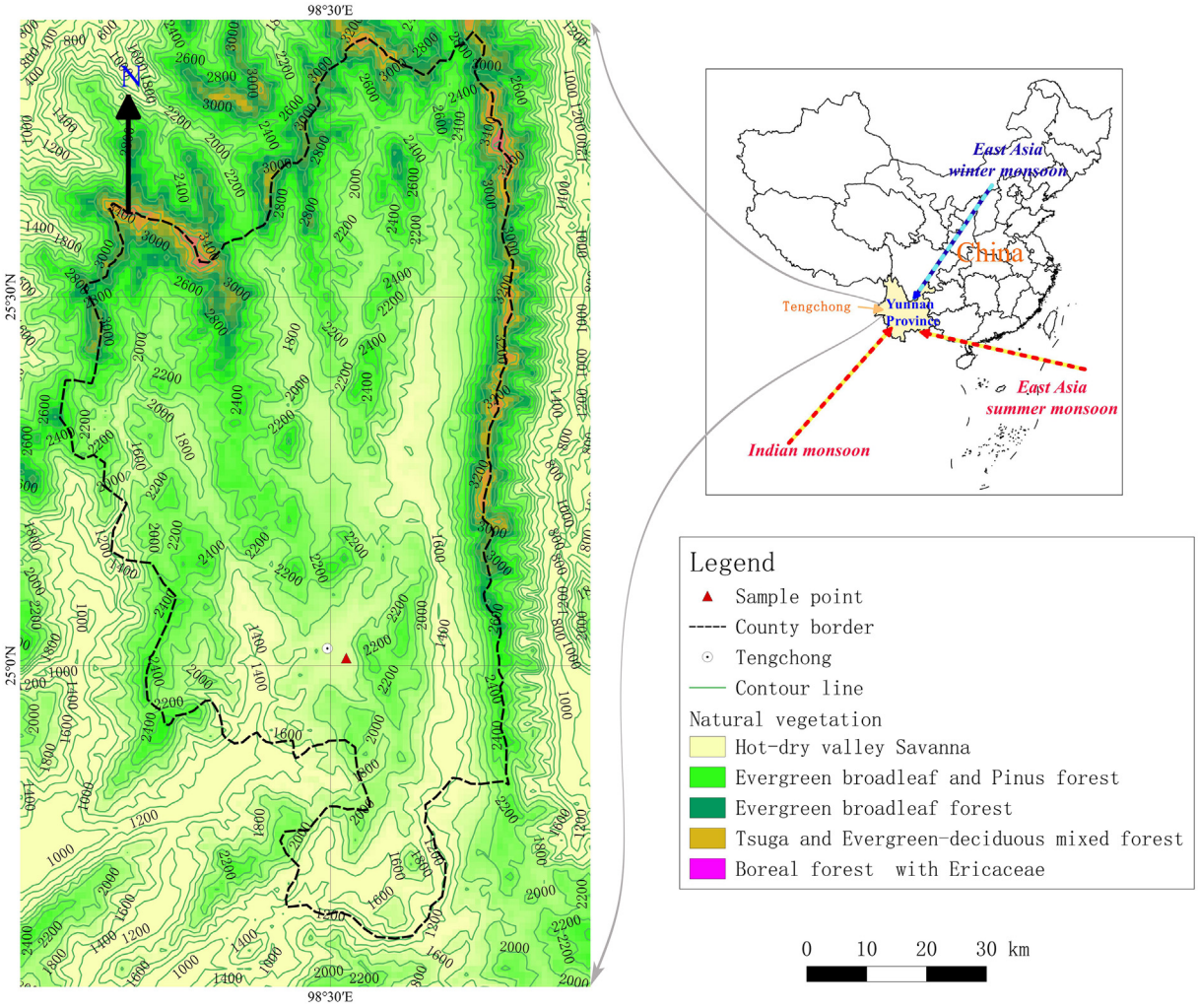

Fig. 1. Modern potential natural vegetation of Tengchong (drawn using Qgis 3.0; elevation data are from the Global Multi-resolution Terrain Elevation Data 2010, https://lta.cr.usgs.gov/GMTED2010).

account for 33.2% on average, while herbs account for 15.9%, fern spores for 50.7%, and algae for 0.2%.

In Zone II-b (369–270 cm; 44.9–29.8 ka), microfossil concentrations increased from bottom to top with an average of 3428 grains/g. The microfossil assemblage of this zone is Monolete spores–Poaceae–*Aster* type–*Pinus*. Trees and shrubs account for an average of 32.1%, while herbs account for 38.9%, fern spores for 28.0%, and algae made up 1.0% of the assemblage.

In Zone II-c (269–207 cm; 29.8–21.8 ka), microfossil concentrations decreased from bottom to top with an average of 1636 grains/g. The microfossil assemblage of this zone is Cyperaceae–*Pinus*–Monolete spores–Poaceae. Trees and shrubs account for 33.9% on average, while herbs account for 51.1%, fern spores for 14.4%, and algae for 0.5%.

In Zone III-a (206–101 cm; 21.8–15.4 ka), microfossil concentrations varied greatly with an average of 3222 grains/g. This zone is characterized by an assemblage of Monolete Spores–*Aster* type–*Taraxacum* type–*Geranium*. Trees and shrubs account for an average of 19.0%, while herbs account for 22.1%, fern spores for 58.8%, and algae for 0.1%.

In Zone III-b (100–46 cm; 15.4–11.8 ka), microfossil concentrations decreased from bottom to top with an average of 4300 grains/g. The microfossil assemblage in this zone is Monolete spores–*Polygonum*–*Tsuga*–*Hygrophila*. Trees and shrubs account for an average of 25.9%, while herbs account for 24.6%, fern spores for 49.5%, and algae for 0.1%.

4.3. Diagram of different microfossil groups

Fig. 3 provides an overview of selected microfossil types and the dominant types in each interval. Surface soil studies in SW China suggest that the microfossil assemblages represent the native vegetation on a basic level, but not completely so (Tao et al., 2010). Because different pollen and spores have distinct production and dispersal methods, meaning that the relationship between microfossils present in an ancient assemblage and the original plant communities is complex (Xiao et al., 2011). For example, the pollen dispersal distance of woody plants is sometimes large, and therefore the pollen might be present in sediments but arise from a catchment area (Yu et al., 2004). Conversely, much herbaceous pollen tends to be dispersed over short distances, and thus its presence in an assemblage better represents the vegetation conditions in situ (Balme, 1995). Fern spores usually have a short transmission distance, but can also be widely spread (Sun et al., 1999). Account for these differences, it is necessary to separately analyze the microfossil types of different groups. Therefore, the percentages of pollen or spores inside their groups in each sample were recalculated and an improved microfossil diagram was created (Fig. 4). For example, the percentage of *Pinus* = *Pinus* pollen / all woody pollen × 100%; the percentage of Poaceae = Poaceae pollen / all herbaceous pollen × 100%; the percentage of Trilete spores = Trilete spores / all fern spores × 100%. This innovative diagram shows the variety of microfossil types more clearly than the traditional diagram (Fig. 3).

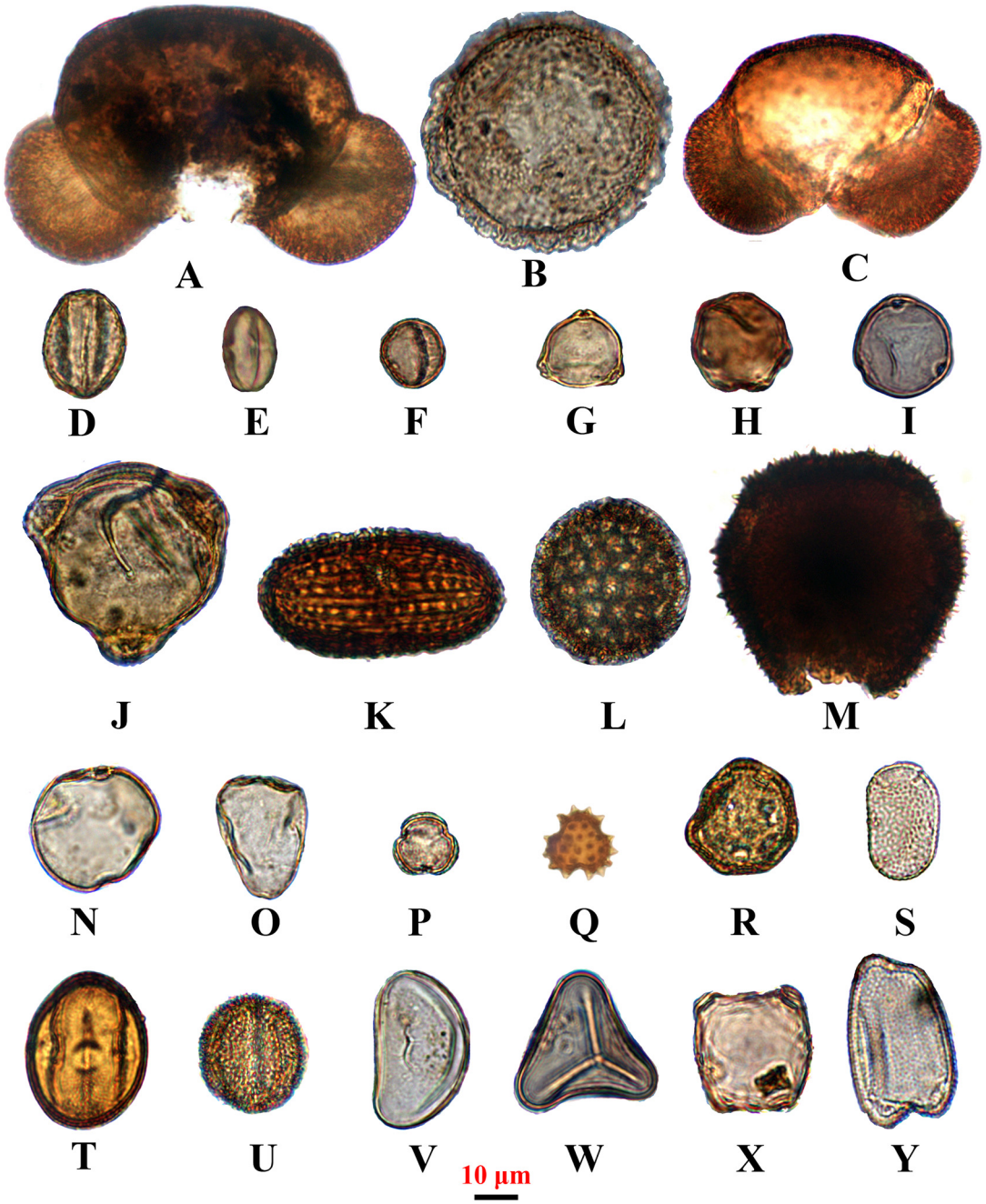

Fig. 2. Photomicrographs of selected pollen types. A. *Abies*; B. *Tsuga*; C. *Picea*; D. *Quercus*; E. *Lithocarpus* or *Castanopsis*; F. *Cyclobalanopsis*; G. *Betula*; H. *Juglans*; I. *Carya*; J. Onagraceae; K. *Hygrophila*; L. *Polygonum* sp.1.; M. *Geranium*; N. Poaceae; O. Cyperaceae; P. *Artemisia*-type; Q. *Aster*-type; R. Caryophyllaceae; S. *Impatiens*; T. *Polygonum* sp.2.; U. *Gentiana*; V. Monolete spores; W. Trilete spores; X. *Mougeotia*; Y. *Spirogyra*.

4.4. Ordination of microfossil data

Ordinationis a type of multivariate analysis, and is useful in exploratory data analysis (Gauch, 1982). It has been widely used in modern and fossil pollen analysis to reveal links between taxa and environmental factors (Behling et al., 2005; Ledger et al., 2017). Here we use this method to explore the ecological significance of the microfossils in Tengchong.

First, to determine whether linear or unimodal-based numerical methods of ordination are suitable, detrended correspondence analysis (DCA) was performed (Hill and Gauch, 1980; Jackson and Somers, 1991) and the results are shown in Table 1. The gradient length of Axis 1 (2.584) is < 4, indicating that the species response in Tengchong is moderately linear (Jongman et al., 1995). Hence, it is valid to use principal component analysis (PCA), an ordination method based on a linear model, to analyze microfossil data (Jolliffe and Cadima, 2016; Prsøch-Danielsen and Simonsen, 1988; Xu et al., 2010).

The PCA results show that Axis 1 and Axis 2 explain 39.9% and 10.1% of environmental variability, respectively (Table 2). In the PCA diagram (Fig. 5), the samples were grouped according to the chronological results, and the results show that the samples of different phases are distinct.

5. Environmental succession and hypotheses mechanisms

5.1. Ecological significance of microfossil types and interpretation of PCA

Algae such as *Spirogyra* and *Mougeotia* provide evidence of a humid

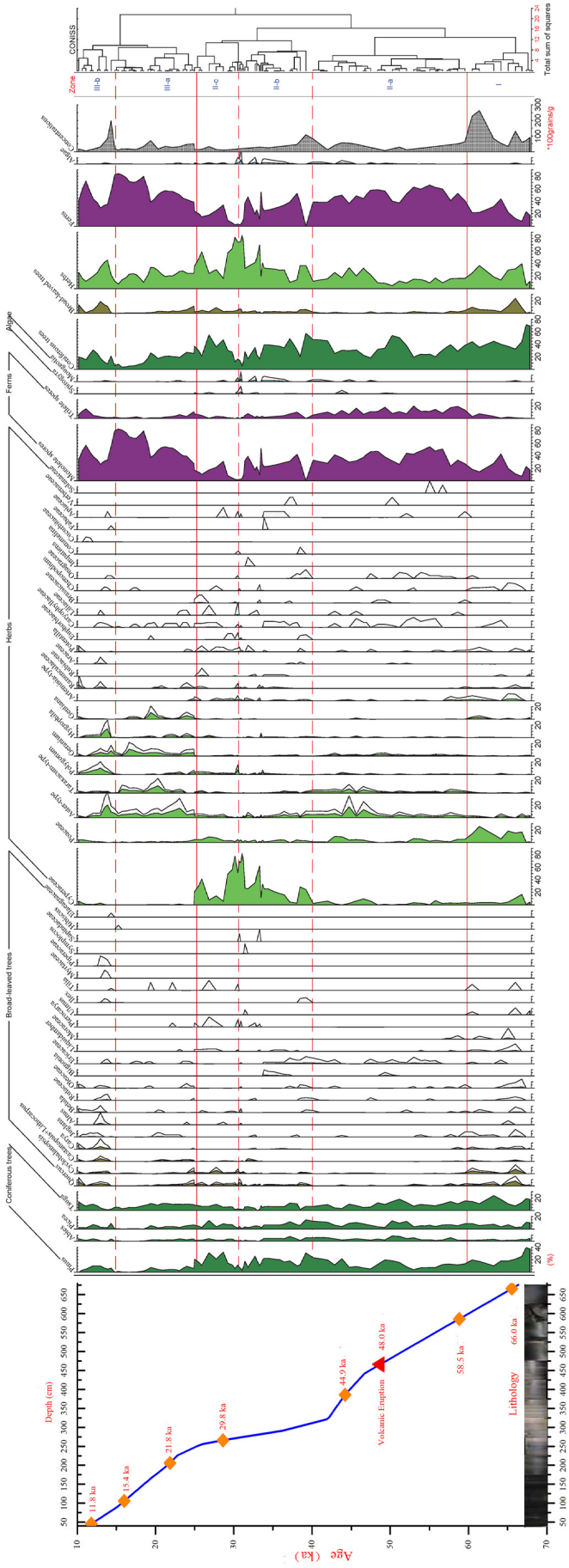

Fig. 3. Microfossil diagram for the Tengchong Core. Percentages of microfossils are calculated regardless of groups, and rare types such as *Carya*, *Juglans*, etc. are magnified. The age model is from Xu et al. (2016), and the pink triangles and blue circles represent ^{14}C ages and OSL ages respectively. (For interpretation of the references to colour in this figure legend, the reader is referred to the web version of this article.)

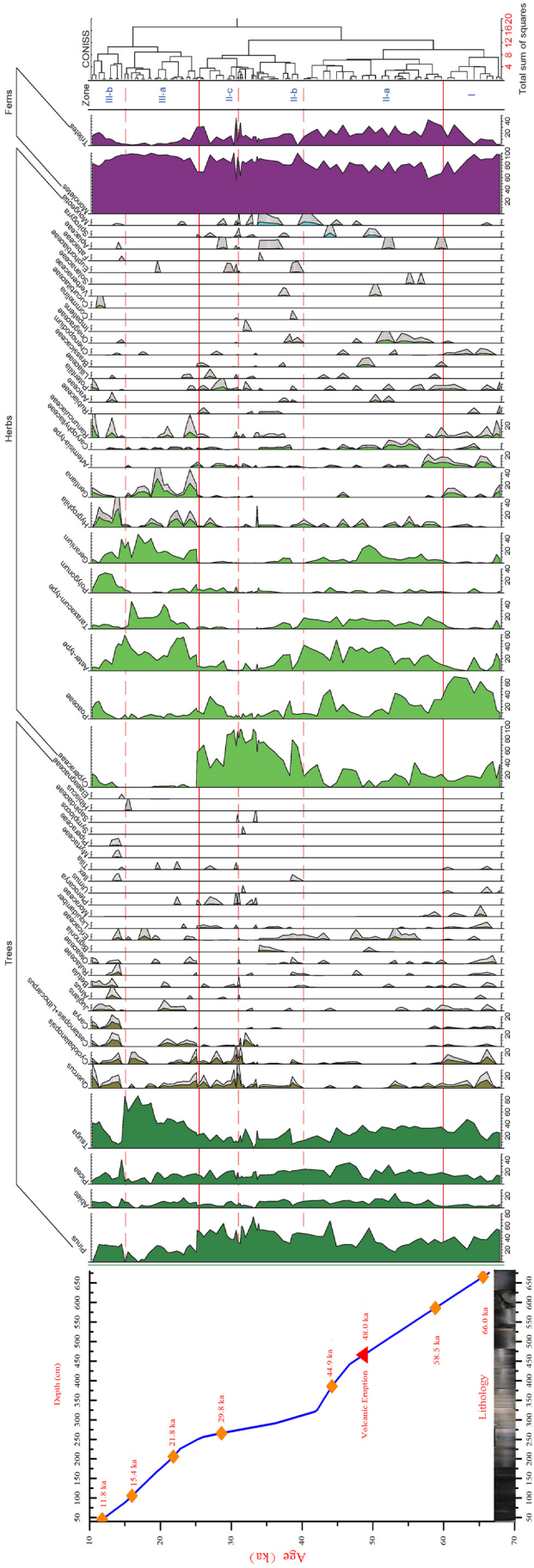

Fig. 4. Microfossil diagram for the Tengchong Core. Percentages of microfossils within groups of Trees, Herbs, and Ferns are calculated separately. The age model is from Xu et al. (2016), and the pink triangles and blue circles represent ^{14}C ages and OSL ages, respectively. (For interpretation of the references to colour in this figure legend, the reader is referred to the web version of this article.)

Table 1
Axes values of DCA.

Axes	1	2	3	4	Total inertia
Eigenvalues	0.415	0.103	0.044	0.031	1.126
Lengths of gradient	2.584	1.220	1.339	1.523	
Cumulative percentage variance	36.9	46.0	49.9	52.6	
Sum of all eigenvalues					1.126

Table 2
Axes values of PCA.

Axes	1	2	3	4	Total variance
Eigenvalues:	0.399	0.101	0.091	0.072	1.000
Cumulative percentage variance	39.9	50.0	59.1	66.3	
Sum of all eigenvalues					1.000

environment (Li et al., 2016; Zhu et al., 2013) and Cyperaceae are also typical plants in wetlands (Zhu et al., 2010); therefore, the presence of both points to a moist environment. In contrast, *Aster*-type, *Taraxacum*-type, and *Geranium* are common herbs in arid and semi-arid regions (Illyés et al., 2007; Wang et al., 2005; Zhao and Herzschuh, 2009), meaning they can be used to indicate dry conditions. Considering the growth environment of the above types, it is reasonable to use Axis 1 in the PCA to represent precipitation. The water level in the Tengchong wetlands correlates with both temperature and precipitation because evaporation increases as temperature rises.

Abies and *Picea* plants live in cold and wet environments and they are generally found at high latitudes and in low-latitude alpine areas in China. According to fossil records, *Abies* and *Picea* had larger distribution ranges during Quaternary glacial periods than the present, so they can be seen as evidence of climate cooling (Liu et al., 2002; Xiang et al., 2007; Binney et al., 2009). Correspondingly, Fagaceae taxa such as *Quercus*, *Cyclobalanopsis*, and *Lithocarpus/Castanopsis* are common components of subtropical forests and temperate forests, indicating warmer climates (Ni and Song, 1997; Liu and Hong, 1998; Zhou, 1992). Therefore, the main ecological factor represented by Axis 2 in PCA can be considered as a temperature gradient.

5.2. History of climate and vegetation evolution

The pollen present at Tengchong indicates that *Pinus*, *Tsuga*, *Abies*, and *Picea* were present from 66.0 to 11.8 ka. This suggests that the vegetation around the sampling sites was dominated by subtropical coniferous forest, similar to modern vegetation. The main herb pollen types such as Cyperaceae, Poaceae, *Geranium*, *Hygrophila*, *Gentiana*, and Onagraceae are commonly seen in modern wetlands in Tengchong (Shen and Liang, 2005). The dominant types of herb pollen are variable at different stages, suggesting that wetland type shifts with changing climate. The vegetation and climate of each stage is described below based on the microfossil assemblages and the climatic inferences are derived from the PCA.

5.2.1. MIS 4 (66.0–58.5 ka)

During the interval corresponding to MIS 4, the percentages of

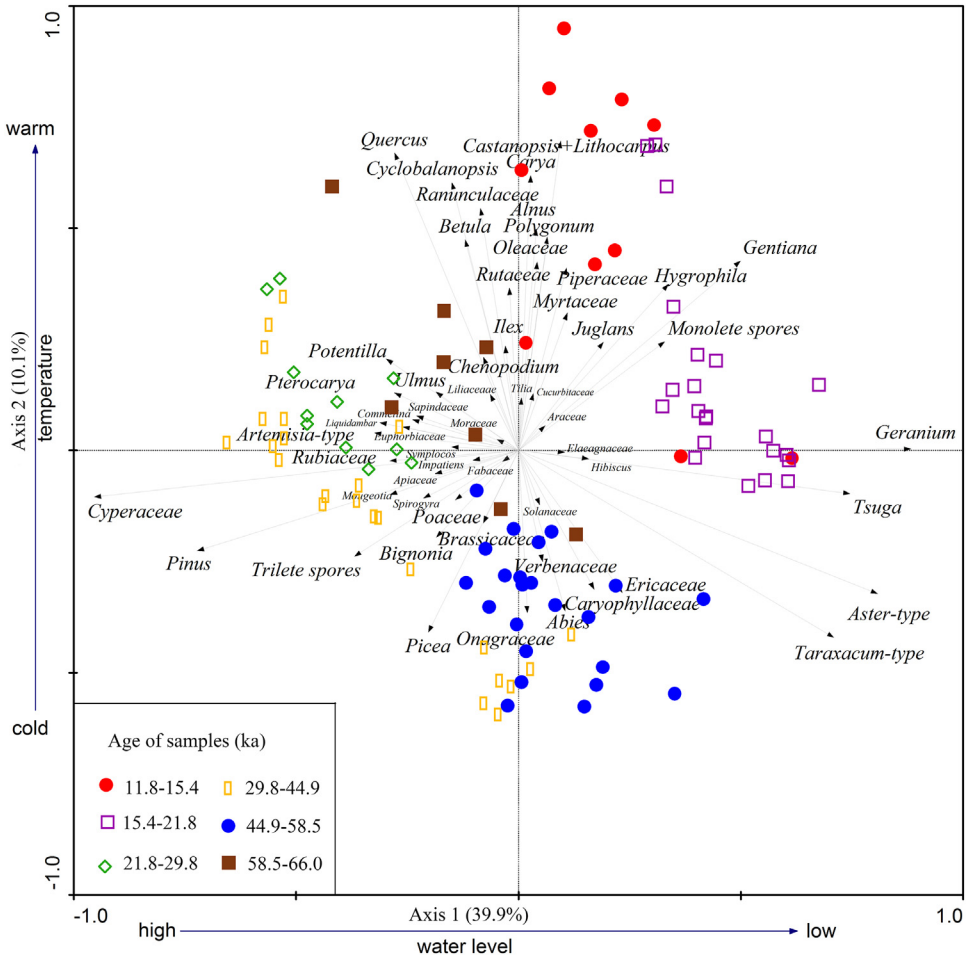

Fig. 5. Principal component analysis of microfossil and samples in the Tengchong Core. (For interpretation of the references to colour in this figure, the reader is referred to the web version of this article.)

broadleaf pollen, especially *Quercus* and *Cyclobalanopsis*, are relatively high. Herb pollen mainly consisted of Poaceae, Cyperaceae, *Aster*-type, and *Artemisia*-type. According to modern meadow vegetation in Yunnan Province, this assemblage can be classified as sub-alpine meadow due to the dominance of Poaceae. This kind of meadow is distributed at elevations of ~3000 m today (Wu et al., 1987), indicating that the climate during MIS 4 was cooler than present. Down-core concentrations of fern spores are strongly correlated with strong hydrodynamics forces (Hooghiemstra et al., 2006). Fern spores are clearly less abundant in this period, which may be due to lower water levels.

As the PCA results show, most of the samples (brown squares in Fig. 5) in this stage are distributed in moderate temperature and moderate precipitation intervals, suggesting that water levels were relatively low under cool and semi-humid climatic conditions, which can also be inferred from the lithology of the peat.

5.2.2. MIS 3c and MIS 3b (early and middle stages of MIS 3, 58.5–44.9 ka)

Pollen from *Abies* and *Picea*, which favor cold climates, significantly increase in the depth intervals corresponding to MIS 3c and MIS 3b, while broadleaf pollen content decreases. The appearance of Ericaceae pollen, which is typical of elevations higher than 4000 m (Ming and Fang, 1979), also indicates a decrease in temperature. The major herb components are *Aster*-type, *Taraxacum*-type, Poaceae, Cyperaceae, and *Geranium*, which are similar to the muddy beach sparse meadows distributed at about 4000 m in Yunnan today (Wu et al., 1987). Therefore, the distribution elevation of this meadow type is ~1000 m higher than that inferred for MIS 4, indicating that the temperature during MIS 3c and MIS 3b might have been about 6 °C lower than in MIS 4. In addition, the higher herb species diversity, which is also related to higher altitude (Xu et al., 2008), can be taken as evidence of cooling. The percentage of fern spores are significantly higher in this interval, which may be linked to a rise in water level, and subsequent transportation of spores in the surrounding vegetation to the sampling sites where they become relatively enriched.

According to the PCA results, most of the samples in this interval (blue circles in Fig. 5) are distributed in lower-temperature and moderate-precipitation intervals, indicating that the climate was cold and semi-humid. Although there were no significant differences in precipitation, the significantly lower temperature would have led to reduced evaporation, which may be the main reason that the lithology suggests a lacustrine environment.

5.2.3. MIS 3a (late stage of MIS 3, 44.9–29.8 ka)

In this interval, the *Abies* and *Picea* contents remain high relative to the previous zone, the *Tsuga* content decreased while *Pinus* content increased, Ericaceae is still present and the broadleaf pollen content remains low, thus suggesting no significant changes in forest vegetation. *Pinus* pollen can travel great distances (Wu and Xiao, 1989), whereas the transmission distance of *Tsuga* is much shorter (Jackson and Lyford, 1999). Therefore, an increase in atmospheric circulation could have been responsible for the greater proportion of *Pinus* pollen amongst the woody taxa. The Cyperaceae content increases rapidly amongst the herbaceous plants, while Poaceae, *Aster*-type, and *Taraxacum*-type pollen components gradually decrease. The community structure is similar to a modern sedge swamp meadows, which are distributed today between 3200 and 4100 m asl (Wu et al., 1987), indicating that temperatures were still cool but a little warmer than in MIS 3c and MIS 3b. The proportion of fern spores decreases in association with an increase in Cyperaceae pollen. In addition, two types of algae (*Mougeotia* and *Spirogyra*) appear in this stage (Mann et al., 1988; Schindler et al., 1990), which also supports the idea of high water levels at that time. The increase in precipitation during this period had been deemed as the result of enhanced ISM intensity (Shi et al., 2001).

There is a significant change in microfossil content at a depth of 370 cm (45 ka). The amount of *Tsuga*, *Abies*, *Aster*-type, *Taraxacum*-type, Trilete spores, and Cyperaceae increases abruptly, indicating a cold event. The timing of this event is consistent with Heinrich 5 (van Meerbeeck et al., 2009). Similarly, Heinrich 4, and Heinrich 3 can also be recognized in MIS 3a.

The temperature ranges inferred from the PCA results (orange rectangles in Fig. 5) are wide in this stage, indicating that climate variability intensified. Precipitation significantly increased compared with the previous stage, and so water levels would also have increased, and the sediments were mostly lake deposits.

5.2.4. Early phase of MIS 2 (29.8–21.8 ka)

The percentage of coniferous pollen is slightly lower in the early MIS 2 depth interval, while the percentage of broadleaf pollen such as *Quercus*, *Cyclobalanopsis*, *Lithocarpus/Castanopsis*, and *Pterocarya* is relatively high, indicating that both subtropical coniferous forest and subtropical broad-leaved forests were present in the surrounding vegetation at this time. Herb plants are still dominated by Cyperaceae and Poaceae (other herbs are significantly reduced) and species diversity is lower than in the previous interval. The vegetation type appears to be the typical sedge swamp meadow. The algae *Mougeotia* and *Spirogyra* are reduced, indicating a fall in water level in this phase.

According to PCA results (green diamonds in Fig. 5), precipitation in the early MIS 2 was relatively high, but the temperature had also increased, so the water level decreased as evaporation increased compared with the previous period. Therefore, the sediments in this phase turned into peats.

5.2.5. LGM (21.8–15.4 ka)

Abies and *Picea* contents are not significantly different in this intervals compared with those of the previous period. The *Tsuga* content increases while that of *Pinus* decreases gradually and broadleaf pollen contents do not change significantly. Therefore, it is assumed that the main forest vegetation over the LGM was similar to that in MIS 3a. The relative changes in *Tsuga* and *Pinus* content over this interval show opposing trends to those seen in MIS 3c and MIS 3b. Therefore, it can be suggested that during this period, atmospheric circulation was gradually weakened, resulting in a reduced *Pinus* content. Amongst the herb pollen, Cyperaceae almost disappears in this interval, replaced by an increase in *Aster*-type, *Taraxacum*-type, *Geranium* and *Gentiana*. These plants are terrestrial herbs and indicate a significant decline in water level. The species composition of herb land is similar to that of the modern subtropical meadow distributed at ~3000 m (Wu et al., 1987), resembling the vegetation type inferred for MIS 4, and thus cooler than today. At this stage, the water level was reduced and the hydrodynamics was very weak, but the fern spores, especially the Monolete spores, significantly increased in abundance, indicating that the ferns are mostly part of the meadow. Algae almost disappeared at this stage, consistent with a decline in water level. The reduction in precipitation during the LGM is probably related to the weakening of ISM (Pausata et al., 2011; Yang et al., 2016).

At the beginning of this phase (i.e., the MIS 3a–MIS 2 transition), a sudden decline in *Pinus* and Cyperaceae may indicate a general cooling climate; the age of this (24 ka) is comparable to the cold event Heinrich 2 (Gutjahr and Lippold, 2011).

The PCA-inferred temperatures for this stage (samples represented by purple squares in Fig. 5) were not significantly different from those for the previous stage, but precipitation was significantly lower. As a result, the water level would have decreased significantly and this would explain the transition from lacustrine muds to peat.

5.2.6. The Last Deglaciation (15.4–11.8 ka)

In this interval, pollen diversity amongst woody plants is significantly higher than in the older intervals. Temperate-subtropical components such as *Quercus*, *Cyclobalanopsis*, *Betula*, and Rutacaeae that are found today at lower altitudes either appear or increase significantly in abundance, indicating that the temperature was higher

than before. The subtropical broad-leaved forest expanded from low to high altitudes. It is noteworthy that in an early part of this phase, there is a sharp increase in *Picea* and *Abies* while *Tsuga* contents declined, indicating a cooling at ~15 ka, perhaps corresponding to Heinrich 1, which is also recognized in Qinghai lake (Xiao et al., 2016). In the early stages of this interval, the herbs are mainly *Aster*-type, *Geranium* and *Hygrophila*. In the middle stage, *Polygonum* was dominant and at the end of this phase, Poaceae, Cyperaceae, *Gentiana* and Ranunculaceae became dominant, indicating that the in situ vegetation changes from forbs meadow to grass meadow. At this stage, the water level was low, and the ferns mainly occurred as part of the meadow. The fern spore content increased and then declined, reflecting a possible increase and then decrease in temperature, perhaps corresponding to the Bølling–Allerød warm period and the Younger Dryas cold event (Zhang et al., 2015; Xiao et al., 2016).

As the PCA results show (red circles in Fig. 5), precipitation was slightly higher in this stage but remained at a relatively low levels. The inferred temperature was also significantly higher for samples in this interval than in the previous, with values reaching the highest of the whole section. An associated increase in evaporation may have led to a further decrease in the water level, but it remained wet enough to sustain a wetland. Yang et al. (2016) contended that the climate in the Tengchong Basin at 15.8–12.8 ka was dry and slightly colder than in later intervals, implying that although the last deglaciation was the warmest stage of the Last Glaciation interval, as inferred from the pollen records in this study, it was still cooler than present.

5.3. Comparison with geochemical indicators and related regions

The percentages of *Abies* and *Picea* amongst the woody pollen (hereafter referred to as APWP) were compared with the percentages of broadleaf type woody taxa and the following parameters: PCA Axis 1 (precipitation), PCA Axis 2 (temperature), humification, bulk density and magnetic susceptibility in the Tengchong peat core, grain size in Qilu Lake, solar insolation, and Chinese stalagmite $\delta^{18}O$ records (Hodell et al., 1999; Wang et al., 2008; Xu et al., 2016) (Fig. 6). Heinrich events 1–5 (Zhou et al., 2008) can be clearly seen in the pollen record variations, where they are characterized by an increase in APWP and a decrease in the broadleaf types of woody pollen. Xiao et al. (2016) attributed the decline of fire events at ~15 ka in Tengchong to increased humidity; which fits the records revealed in PCA Axis 1.

Down-core changes in magnetic susceptibility generally follow changes in APWP. However, they are in the opposite direction around 48 ka, which corresponds to a volcanic eruption interval, where the increase of APWP corresponds to a decrease of magnetic susceptibility. This suggests that the volcanic eruption may have caused a cooling event and a magnetic abnormality in the sediment.

Bulk density is an effective indicator of climate change. For lake sediments in tropical and subtropical areas, a higher bulk density generally indicates a colder climate (Liu et al., 2000). Therefore, we can infer that temperatures in the Tengchong Basin area during MIS 3c and MIS 3b were lower than in MIS 3a, which is consistent with the microfossil data. Peat forms rapidly under warm climates, resulting in less compact sediments with lower bulk densities (Yu et al., 2003; Zhao et al., 2011b). Conversely, high bulk density in peaty sediments suggests formation under colder climates. Temperatures inferred from bulk density and microfossils are in good agreement between MIS 4 and LGM.

The climatic significance of humification is inconsistent between different regions. In some areas, a high degree of humification is indicative of a warm climate, while low degrees of humification suggest formation under cold climates. Conversely, in other areas this pattern is reversed with low degrees of humification linked to warmer temperatures (Ma et al., 2009; Chen et al., 2014). Studies of peat in the eastern margin of the Qinghai-Tibet Plateau (Wang et al., 2004; Xu et al., 2013) suggest that a high degree of humification represents peat formation under higher precipitation and temperatures regimes. Considering that the Tengchong Basin is close to the above area and the local terrain, precipitation patterns, and vegetation are similar, we consider that the degree of humification in the study area is also positively correlated with precipitation and temperature and this is consistent with the microfossil results.

Stable oxygen isotope ratios ($\delta^{18}O$) in speleothems are related both to temperature and to precipitation. Studies of $\delta^{18}O$ values in modern precipitation in SW China (Li et al., 2017) suggest that $\delta^{18}O$ values are mainly negatively affected by precipitation and therefore any temperature effect may be masked by precipitation effects. It can therefore be inferred that the $\delta^{18}O$ curve in Fig. 6 mainly reflects changes in precipitation. However, the $\delta^{18}O$ curve for the interval between the LGM and the Last Deglaciation is probably an exception and is more likely to be related to temperature as the precipitation was low.

The median grain size of sediments can be used as an indicator of winter monsoon strength (Jiang and Ding, 2010; Xiao et al., 1995) or changes in lake level (Li et al., 2009; Xiao et al., 2013). Hodell et al. (1999) categorized the 38–63 μm sediment fraction in Qilu Lake (also in Yunnan Province) as aeolian in origin, and linked it with changes in the intensity of winter monsoon winds and/or local aridity. As the grain size curve shows, although the area experienced drought conditions during the LGM, the accumulation rate for the > 38 mm grain size fraction was not higher during this interval compared to MIS 3. Therefore, we can speculate that the winter monsoon during the LGM in SW China was not very strong. However, a study of loess in Northwest China (Chen et al., 1997) suggests it was the opposite there; i.e., that the winter monsoon during the LGM was stronger than in MIS 3. Therefore, the winter monsoon in SW China appears to show characteristics that differ with other regions in China.

On orbital time scales, solar radiation (insolation) is considered to be a major control on changes in past monsoon intensity (Leuschner and Sirocko, 2003). However, according to an investigation of sediments in the Bengal Fan, the intensity of the ISM is not strictly synchronized with insolation after MIS 4, right after the volcanic eruption event associated with the Younger Toba Tuff (Weber et al., 2018). The changes of the ISM may have further affected the subsequent climate of SW China. During the LGM, annual sea surface temperatures in the Bay of Bengal fell by only about 1 °C compared with modern temperatures (Trend-Staid and Prell, 2002; Annan and Hargreaves, 2013). Consequently, although the ISM during LGM was weaker than present, it might still have been relatively strong.

Multiple studies suggest that ice advance events happened during MIS 3 in SW China, and that glaciers during MIS 3 were equivalent in size to or even larger than those of the LGM (Shi and Yao, 2002; Zhao et al., 2007; Zhang and Liu, 2014). Scholars have generally attributed the ice advance during MIS 3 to the higher precipitation and relatively low temperatures according to the $\delta^{18}O$ curve, but have not considered that temperatures during MIS 3 may have been lower than the LGM (van Meerbeeck et al., 2009; Han et al., 2010). Chen et al. (2014) studied pollen and grain size records of Xingyun Lake over the interval 36.4–13.4 ka, and inferred that the coldest stage within this period was the LGM, but they did not have data from earlier periods. As mentioned above, the relationship between $\delta^{18}O$ values in sediment archives and precipitation/temperature is complex and sometimes it cannot be accurately determined whether peaks in the $\delta^{18}O$ curve were caused by changes in temperature or precipitation or some combination of the two. Under these circumstances, microfossil analyses are helpful in distinguishing the influences of temperature and precipitation. The *Abies* and *Picea* pollen curves, the broadleaf pollen curve, and the main microfossil assemblages all indicate that during MIS 3 there existed a colder phase than the LGM in SW China, despite the fact that solar insolation in MIS 3 might have been more intense.

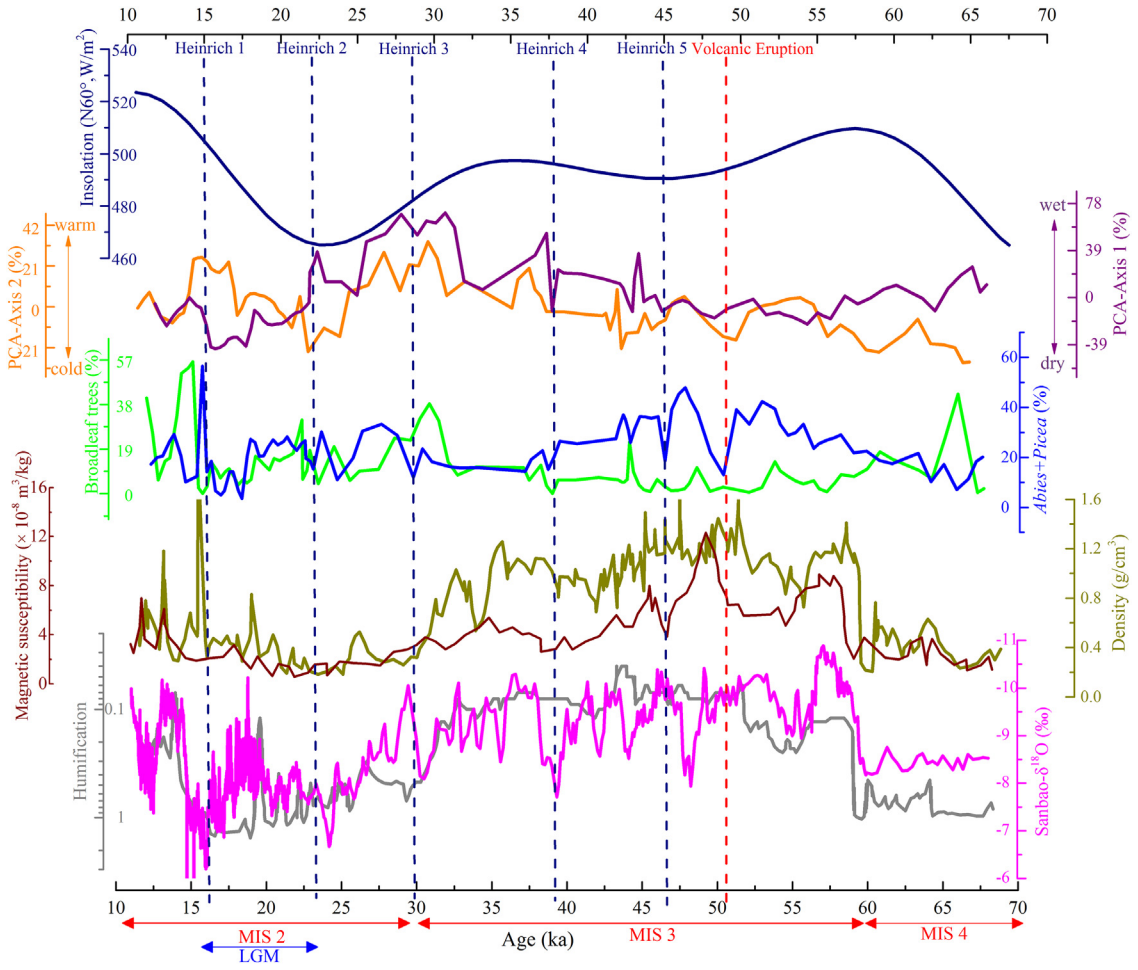

Fig. 6. Comparison between the percentages of *Abies* and *Picea* amongst the woody pollen versus other indices. *Abies* and *Picea* pollen (blue), broadleaf tree pollen (green), PCA-Axis 1 (purple), and PCA Axis 2 (orange) are based on microfossil data in this study; solar insolation at 60° N latitude (dark blue) is after Berger (1978); accumulation rates for grains with sizes > 38 μm in Qilu Lake (black) are redrawn from Hodell et al. (1999); magnetic susceptibility (red brown), bulk density (yellow brown), and humification (grey) are after Xu et al. (2016); Sanbao-$\delta^{18}O$ (pink) is after Wang et al. (2008). (For interpretation of the references to colour in this figure legend, the reader is referred to the web version of this article.)

6. Conclusions

The evolution of vegetation and climate during the Last Glaciation in Tengchong Basin was reconstructed using a palynological approach. Concentrations of woody taxa pollen, herb taxa pollen, fern spores, and algae in Tengchong Basin sediments show clear changes through the different periods of the Last Glaciation. These vegetation changes can be interpreted as the result of climatic changes as follows. During the Last Glaciation Tengchong was generally colder than today, similar to other parts of China. Heinrich events 1–5 and a volcanic eruption event can be recognized in the pollen records. Our results also imply that the LGM may have not been the coldest period during the Last Glaciation in Tengchong; in this region, it appears that MIS 3 not only had higher precipitation, but also might have included phases colder than the LGM.

This study strongly supports the idea put forward in other studies that climatic changes during the Last Glaciation in SW China were different to those in eastern China. The unique changes in climate and vegetation seen in Tengchong Basin during the LGM are likely to have been caused by a combination of a relatively weaker winter monsoon and a relatively strong ISM, but may also relate to the local terrain. Further work is necessary to determine which factor is more important.

Acknowledgments

This work was funded by the National Natural Science Foundation of China (No.: 41672169; 41473120), and by the University of Chinese Academy of Sciences Joint PhD Training Program (UCAS(2015)37) Joint PhD Training Program. We are grateful to Bas van Geel (University of Amsterdam) for identifying the algae in the samples. Some pollen types were identified with the help of Limi Mao and Junwu Shu (Nanjing Institute of Geology and Paleontology, Chinese Academy of Sciences). Weiming Wang (Nanjing Institute of Geology and Paleontology, Chinese Academy of Sciences) provided advice on the age division of the Last Glaciation. Yiman Fang (University of Hull) offered assistance on the Principal Component Analysis of pollen. We would also like to thank the reviewers for their valuable comments and efforts to improve the manuscript.

References

Annan, J.D., Hargreaves, J.C., 2013. A new global reconstruction of temperature changes at the last Glacial Maximum. Clim. Past 9, 367–376.
Balme, B.E., 1995. Fossil in situ spores and pollen grains: an annotated catalogue. Rev. Palaeobot. Palynol. 87, 81–323.
Bates, C.D., Coxon, P., Gibbard, P.L., 1978. A new method for the preparation of clay-rich sediment samples for palynological investigation. New Phytol. 81, 459–463.
Behling, H., Pillar, V.D., Bauermann, S.G., 2005. Late Quaternary grassland (Campos), gallery forest, fire and climate dynamics, studied by pollen, charcoal and multivariate analysis of the São Francisco de Assis core in western Rio Grande do Sul (southern Brazil). Rev. Palaeobot. Palynol. 133, 235–248.
Berger, A.L., 1978. Long-term variations of daily insolation and Quaternary climatic changes. J. Atmos. Sci. 35, 2362–2367.
Binney, H.A., Willis, K.J., Edwards, M.E., Bhagwat, S.A., Anderson, P.M., Andreev, A.A.,

Blaauw, M., Damblon, F., Haesaerts, P., Kienast, F., 2009. The distribution of Late-Quaternary woody taxa in northern Eurasia: evidence from a new macrofossil database. Quat. Sci. Rev. 28, 2445–2464.
Brush, G.S., DeFries, R.S., 1981. Spatial distributions of pollen in surface sediments of the Potomac estuary. Limnol. Oceanogr. 26, 295–309.
Chen, F., Bloemendal, J., Wang, J., Li, J., Oldfield, F., 1997. High-resolution multi-proxy climate records from Chinese loess: evidence for rapid climatic changes over the last 75 kyr. Palaeogeogr. Palaeoclimatol. Palaeoecol. 130, 323–335.
Chen, X., Chen, F., Zhou, A., Huang, X., Tang, L., Wu, D., Zhang, X., Yu, J., 2014. Vegetation history, climatic changes and Indian summer monsoon evolution during the Last Glaciation (36,400–13,400 cal yr BP) documented by sediments from Xingyun Lake, Yunnan, China. Palaeogeogr. Palaeoclimatol. Palaeoecol. 410, 179–189.
Ehlers, J., Gibbard, P.L., Hughes, P.D., 2004. Quaternary Glaciations: Extent and Chronology. Part I: Europe. Episodes 31. pp. 139–140.
Fu, C., Jiang, Z., Guan, Z., He, J., Xu, Z., 2008. Regional Climate Studies of China. Springer, Berlin Heidelberg.
Gauch, H.G., 1982. Multivariate analysis in community ecology. Q. Rev. Biol. 1, 652.
Grimm, E.C., 2011. TILIA 1.7. 16: Illinois State Museum. Res. Collect. Cent. pp. 1011.
Gutjahr, M., Lippold, J., 2011. Early arrival of Southern Source Water in the deep North Atlantic prior to Heinrich event 2. Paleoceanography 26.
Ha, K.-J., Seo, Y.-W., Lee, J.-Y., Kripalani, R.H., Yun, K.-S., 2017. Linkages between the South and East Asian summer monsoons: a review and revisit. Clim. Dyn. https://doi.org/10.1007/s00382-017-3773-z.
Han, W., Fang, X., Yang, S., King, J., 2010. Differences between East Asian and Indian monsoon climate records during MIS3 attributed to differences in their driving mechanisms: evidence from the loess record in the Sichuan basin, southwestern China and other continental and marine climate records. Quat. Int. 218, 94–103. https://doi.org/10.1016/j.quaint.2010.01.002.
Helmens, K.F., 2014. The Last Interglacial–Glacial cycle (MIS 5–2) re-examined based on long proxy records from central and northern Europe. Quat. Sci. Rev. 86, 115–143.
Hill, M.O., Gauch, H.G., 1980. Detrended correspondence analysis: an improved ordination technique. In: Classification and Ordination. Springer, pp. 47–58.
Hodell, D.A., Brenner, M., Kanfoush, S.L., Curtis, J.H., Stoner, J.S., Xueliang, S., Yuan, W., Whitmore, T.J., 1999. Paleoclimate of southwestern China for the past 50,000 yr inferred from lake sediment records. Quat. Res. 52, 369–380.
Hooghiemstra, H., Lézine, A.-M., Leroy, S.A.G., Dupont, L., Marret, F., 2006. Late Quaternary palynology in marine sediments: a synthesis of the understanding of pollen distribution patterns in the NW African setting. Quat. Int. 148, 29–44.
Hu, S., Goddu, S.R., Appel, E., Verosub, K., Xiangdong, Y., Wang, S., 2005. Palaeoclimatic changes over the past 1 million years derived from lacustrine sediments of Heqing basin (Yunnan, China). Quat. Int. 136, 123–129.
Hu, S., Goddu, S.R., Herb, C., Appel, E., Gleixner, G., Wang, S., Yang, X., Zhu, X., 2015. Climate variability and its magnetic response recorded in a lacustrine sequence in Heqing basin at the SE Tibetan Plateau since 900 ka. Geophys. J. Int. 201, 444–458.
Huang, Z., Jiang, W., Zhang, W., 2003. Climatic characteristics in tropic areas of China during MIS 3. Quat. Sci. 1, 8.
Illyés, E., Chytrý, M., Botta-Dukát, Z., Jandt, U., Škodová, I., Janišová, M., Willner, W., Hájek, O., 2007. Semi-dry grasslands along a climatic gradient across Central Europe: vegetation classification with validation. J. Veg. Sci. 18, 835–846.
Jackson, S.T., Lyford, M.E., 1999. Pollen dispersal models in Quaternary plant ecology: assumptions, parameters, and prescriptions. Bot. Rev. 65, 39–75.
Jackson, D.A., Somers, K.M., 1991. Putting things in order: the ups and downs of detrended correspondence analysis. Am. Nat. 137, 704–712.
Jiang, H., Ding, Z., 2010. Eolian grain-size signature of the Sikouzi lacustrine sediments (Chinese Loess Plateau): implications for Neogene evolution of the East Asian winter monsoon. Geol. Soc. Am. Bull. 122, 843–854.
Jolliffe, I.T., Cadima, J., 2016. Principal component analysis: a review and recent developments. Phil. Trans. R. Soc. A 374, 20150202.
Jongman, R.H., ter Braak, C.J., van Tongeren, O.F., 1995. Data Analysis in Community and Landscape Ecology. Cambridge University Press, Cambridge.
Kou, X., Ferguson, D.K., Xu, J., Wang, Y., Li, C., 2006. The reconstruction of paleovegetation and paleoclimate in the Late Pliocene of West Yunnan, China. Clim. Chang. 77, 431–448.
Ledger, P.M., Edwards, K.J., Schofield, J.E., 2017. Competing hypotheses, ordination and pollen preservation: landscape impacts of Norse landnám in southern Greenland. Rev. Palaeobot. Palynol. 236, 1–11.
Leuschner, D.C., Sirocko, F., 2003. Orbital insolation forcing of the Indian Monsoon–a motor for global climate changes? Palaeogeogr. Palaeoclimatol. Palaeoecol. 197, 83–95.
Li, Y., Wang, N., Morrill, C., Cheng, H., Long, H., Zhao, Q., 2009. Environmental change implied by the relationship between pollen assemblages and grain-size in NW Chinese lake sediments since the Late Glacial. Rev. Palaeobot. Palynol. 154, 54–64.
Li, S., Li, J., Wu, Z., Yao, J., 2016. Climatic and environmental changes of the Lugu Lake area during the Late Holocene. Acta Geol. Sin. 90, 1998–2012 (in Chinese with English abstract).
Li, Y., Rao, Z., Cao, J., Jiang, H., Gao, Y., 2017. Highly negative oxygen isotopes in precipitation in southwest China and their significance in paleoclimatic studies. Quat. Int. 440, 64–71.
Liu, M., Hong, B., 1998. The distribution of Fagaceae in China and its relationship with climatic and geographic characters. Acta Phytoecol. Sin. 22, 41–50 (in Chinese with English abstract).
Liu, J., Lyu, H., Negendank, J., Mingram, J., Luo, X., Wang, W., Chu, G., 2000. Periodicity of Holocene climatic variations in the Huguangyan Maar Lake. Chin. Sci. Bull. 45, 1712–1717.
Liu, Z., Fang, J., Piao, S., 2002. Geographical distribution of species in genera *Abies*, *Picea* and *Larix* in China. Acta Geograph. Sin. 57, 577–586.
Long, X., Zhang, W., Zhang, H., Ming, Q., Shi, Z., Niu, J., Lei, G., 2015. Lake sediment records on climate change of the Qinghai lake catchment in Southwest China based on wavelet analysis. In: Zeitschrift Für Die Gesamte Staatswiss, pp. 562–565.
Ma, C., Zhu, C., Zheng, C., Yin, Q., Zhao, Z., 2009. Climate changes in East China since the Late-glacial inferred from high-resolution mountain peat humification records. Sci. China Ser. D Earth Sci. 52, 118–131.
Madanes, N., Dadon, J.R., 1998. Assessment of the minimum sample size required to characterize site-scale airborne pollen. Grana 37, 239–245.
Mann, S., Mann, H., Fyfe, W., 1988. Intracellular aragonite crystals in the fresh-water alga, *Spirogyra* sp. Mineral. Mag. 52, 241–245.
Ming, T., Fang, R., 1979. On the origin and geographic distribution of genus *Rhododendron* L. Acta Bot. Yunnanica 2, 2 (in Chinese with English abstract).
Ni, J., Song, Y., 1997. Relationships between geographical distribution of *Cyclobalanopsis glauca* and climate in China. Acta Bot. Sin. 39, 451–460 (in Chinese with English abstract).
Ono, Y., Naruse, T., 1997. Snowline elevation and eolian dust flux in the Japanese islands during isotope stages 2 and 4. Quat. Int. 37, 45–54.
Pausata, F.S.R., Battisti, D.S., Nisancioglu, K.H., Bitz, C.M., 2011. Chinese stalagmite $\delta^{18}O$ controlled by changes in the Indian monsoon during a simulated Heinrich event. Nat. Geosci. 4, 474.
Pearsall, D.M., 2015. Paleoethnobotany. In: A Handbook of Procedures, Third edition. Left Coast Press, Walnut Creek.
Porter, S.C., An, Z., 1995. Correlation between climate events in the North Atlantic and China during the last glaciation. Nature 375, 305–308.
Prsøch-Danielsen, L., Simonsen, A., 1988. Principal components analysis of pollen, charcoal and soil phosphate data as a tool in prehistoric land-use investigation at Forsandmoen, Southwest Norway. Nor. Archaeol. Rev. 21, 85–102.
Schindler, D.W., Beaty, K.G., Fee, E.J., Cruikshank, D.R., DeBruyn, E.R., Findlay, D.L., Linsey, G.A., Shearer, J.A., Stainton, M.P., Turner, M.A., 1990. Effects of climatic warming on lakes of the central boreal forest. Science 967–970.
Shen, L., Liang, L., 2005. Assessment on the resources and environmental situation of plants and animals in Beihai wetland. For. Resour. Manag. 2, 61–67.
Shi, Y., Yao, T., 2002. MIS 3b (54–44 ka BP) cold period and glacial advance in middle and low latitudes. J. Glaciol. Geocryol. 24, 1–9.
Shi, Y., Yu, G., Liu, X., Li, B., Yao, T., 2001. Reconstruction of the 30–40 ka bp enhanced Indian monsoon climate based on geological records from the Tibetan Plateau. Palaeogeogr. Palaeoclimatol. Palaeoecol. 169, 69–83.
Stockmarr, J.A., 1971. Tabletes with spores used in absolute pollen analysis. Pollen Spores 13, 615–621.
Sun, X., Li, X., Beug, H.-J., 1999. Pollen distribution in hemipelagic surface sediments of the South China Sea and its relation to modern vegetation distribution. Mar. Geol. 156, 211–226.
Tao, P., Dai, E., Wu, S., 2010. Relationship between surface pollen and modern vegetation in Southwestern China. J. Mt. Sci. 7, 176–186.
ter Braak, C.J.F., Smilauer, P., 2002. Canoco 4.5: Reference Manual and Canodraw for Windows. User's Guide: Software Form Canonical Community Ordination (Version 4.5). Microcomputer Power, Ithaca NY.
Tian, Z., Jiang, D., 2016. Revisiting last glacial maximum climate over China and East Asian monsoon using PMIP3 simulations. Palaeogeogr. Palaeoclimatol. Palaeoecol. 453, 115–126.
Trend-Staid, M., Prell, W.L., 2002. Sea surface temperature at the Last Glacial Maximum: a reconstruction using the modern analog technique. Paleoceanography 17, 11–17.
van Meerbeeck, C., Renssen, H., Roche, D., 2009. How did marine isotope stage 3 and Last Glacial Maximum climates differ? Perspectives from equilibrium simulations. Clim. Past 5, 33–51.
Wang, F., 1995. Pollen Flora of China. Science Press, Beijing (in Chinese).
Wang, B., Wu, R., Lau, K.M., 2001. Interannual variability of the Asian summer monsoon: contrasts between the Indian and the western North Pacific–East Asian monsoons. J. Clim. 14, 4073–4090.
Wang, H., Hong, Y., Zhu, Y., Hong, B., Lin, Q., Xu, H., Leng, X., Mao, X., 2004. Humification degrees of peat in Qinghai-Xizang Plateau and palaeoclimate change. Chin. Sci. Bull. 49, 514–519 (in Chinese with English abstract).
Wang, Y., Zhao, L., Shao, Y., 2005. Comparative analysis of the drought-resistances for turfgrass and main weeds in the temperate semi-arid region. Chin. J. Ecol. 1, 0 (in Chinese with English abstract).
Wang, Z., Tang, Z., Fang, J., 2007. Altitudinal patterns of seed plant richness in the Gaoligong Mountains, south-east Tibet, China. Divers. Distrib. 13, 845–854.
Wang, Y., Cheng, H., Edwards, R.L., Kong, X., Shao, X., Chen, S., Wu, J., Jiang, X., Wang, X., An, Z., 2008. Millennial-and orbital-scale changes in the East Asian monsoon over the past 224,000 years. Nature 451, 1090.
Weber, M.E., Lantzsch, H., Dekens, P., Das, S.K., Reilly, B.T., Martos, Y.M., Meyer-Jacob, C., Agrahari, S., Ekblad, A., Titschack, J., 2018. 200,000 years of monsoonal history recorded on the lower Bengal Fan-strong response to insolation forcing. Glob. Planet. Chang. 166, 107–119.
Wu, L., Li, X., 2004. Analysis on change of annual precipitation with altitude in high mountain areas. Yunnan Geogr. Environ. Res. 2, 1.
Wu, Y., Xiao, J., 1989. Modern pollen rain on Liangwang Mountain of Chenggong, Yunnan. Acta Bot. Yunnanica 11, 145–153 (in Chinese with English abstract).
Wu, Z., Zhu, Y., Jiang, H., 1987. The Vegetation of Yunnan. Science Press, Beijing (in Chinese).
Xiang, X., Cao, M., Zhou, Z., 2007. Fossil history and modern distribution of the genus *Abies* (Pinaceae). Front. For. China 2, 355–365 (in Chinese with English abstract).
Xiao, J., Porter, S.C., An, Z., Kumai, H., Yoshikawa, S., 1995. Grain size of quartz as an indicator of winter monsoon strength on the Loess Plateau of central China during the last 130,000 yr. Quat. Res. 43, 22–29.

Xiao, X., Shen, J., Wang, S., 2011. Spatial variation of modern pollen from surface lake sediments in Yunnan and southwestern Sichuan Province, China. Rev. Palaeobot. Palynol. 165, 224–234.
Xiao, J., Fan, J., Zhou, L., Zhai, D., Wen, R., Qin, X., 2013. A model for linking grain-size component to lake level status of a modern clastic lake. J. Asian Earth Sci. 69, 149–158.
Xiao, X., Haberle, S.G., Shen, J., Yang, X., Han, Y., Zhang, E., Wang, S., 2014. Latest Pleistocene and Holocene vegetation and climate history inferred from an alpine lacustrine record, northwestern Yunnan Province, southwestern China. Quat. Sci. Rev. 86, 35–48.
Xiao, X., Shen, J., Haberle, S.G., Han, Y., Xue, B., Zhang, E., Wang, S., Tong, G., 2016. Vegetation, fire, and climate history during the last 18,500 cal a BP in south-western Yunnan Province, China. J. Quat. Sci. 30, 859–869.
Xiao, X., Haberle, S.G., Shen, J., Xue, B., Burrows, M., Wang, S., 2017. Postglacial fire history and interactions with vegetation and climate in southwestern Yunnan Province of China. Clim. Past 13, 613–627.
Xu, C., Feng, J., Wang, X., Yang, X., 2008. Vertical distribution patterns of plant species diversity in northern Mt. Gaoligong, Yunan Province. Chinese J. Ecol. 3, 3 (in Chinese with English abstract).
Xu, D., Lu, H., Wu, N., Liu, Z., 2010. 30,000-year vegetation and climate change around the East China Sea shelf inferred from a high-resolution pollen record. Quat. Int. 227, 53–60.
Xu, H., Liu, B., Lan, J., Sheng, E., Che, S., Xu, S., 2013. Holocene peatland development along the eastern margin of the Tibetan Plateau. Quat. Res. 80, 47–54.
Xu, H., Lan, J., Sheng, E., Liu, Y., Liu, B., Yu, K., Ye, Y., Cheng, P., Qiang, X., Lu, F., 2016. Tropical/subtropical peatland development and global CH4 during the Last Glaciation. Sci. Rep. 6.
Yang, Y., Zhang, H., Chang, F., Meng, H., Pan, A., Zheng, Z., Xiang, R., 2016. Vegetation and climate history inferred from a Qinghai Crater Lake pollen record from Tengchong, southwestern China. Palaeogeogr. Palaeoclimatol. Palaeoecol. 461, 1–11.
Yu, Z., Campbell, I.D., Campbell, C., Vitt, D.H., Bond, G.C., Apps, M.J., 2003. Carbon sequestration in western Canadian peat highly sensitive to Holocene wet-dry climate cycles at millennial timescales. Holocene 13, 801–808.
Yu, G., Ke, X., Xue, B., Ni, J., 2004. The relationships between the surface arboreal pollen and the plants of the vegetation in China. Rev. Palaeobot. Palynol. 129, 187–198. https://doi.org/10.1016/j.revpalbo.2004.01.007.
Zhang, Y., 1990. Spore Morphology of Chinese Pteridophytes. Science Press, Beijing (in Chinese).
Zhang, W., Liu, B., 2014. Features of the glaciation during the Last Glaciation in northwestern Yunnan Province. J. Glaciol. Geocryol. 36, 30–37.
Zhang, Z., Zhao, M., Yang, X., Wang, S., Jiang, X., Oldfield, F., Eglinton, G., 2004. A hydrocarbon biomarker record for the last 40 kyr of plant input to Lake Heqing, southwestern China. Org. Geochem. 35, 595–613.
Zhang, E., Sun, W., Zhao, C., Wang, Y., Xue, B., Shen, J., 2015. Linkages between climate, fire and vegetation in southwest China during the last 18.5 ka based on a sedimentary record of black carbon and its isotopic composition. Palaeogeogr. Palaeoclimatol. Palaeoecol. 435, 86–94.
Zhao, Y., Herzschuh, U., 2009. Modern pollen representation of source vegetation in the Qaidam Basin and surrounding mountains, north-eastern Tibetan Plateau. Veg. Hist. Archaeobotany 18, 245–260.
Zhao, J., Zhou, S., Liu, S., 2007. A preliminary study of the glacier advance in MIS3b in the western regions of China. J. Glaciol. Geocryol. 29, 233–241.
Zhao, J., Shi, Y., Jie, W., 2011a. Comparison between Quaternary glaciations in china and the marine oxygen isotope stage (MIS): an improved schema. Acta Geograph. Sin. 66, 867–884.
Zhao, Y., Yu, Z., Zhao, W., 2011b. Holocene vegetation and climate histories in the eastern Tibetan Plateau: controls by insolation-driven temperature or monsoon-derived precipitation changes? Quat. Sci. Rev. 30, 1173–1184.
Zhao, Y., Yu, Z., Tang, Y., Li, H., Yang, B., Li, F., Zhao, W., Sun, J., Chen, J., Li, Q., 2014. Peatland initiation and carbon accumulation in China over the last 50,000 years. Earth-Sci. Rev. 128, 139–146.
Zhen, Z., Zhong, W., Xue, J., Zheng, Y., Liu, W., 2008. Progress in the studies of climatic features in different areas of China during the MIS-3. J. Glaciol. Geocryol. 5, 16.
Zhou, Z., 1992. Origin phylogeny and dispersal of Quercus from China. Acta Bot. Yunnanica 3, 0 (in Chinese with English abstract).
Zhou, H., Zhao, J., Feng, Y., Gagan, M.K., Zhou, G., Yan, J., 2008. Distinct climate change synchronous with Heinrich event one, recorded by stable oxygen and carbon isotopic compositions in stalagmites from China. Quat. Res. 69, 306–315.
Zhu, C., Ma, C., Yu, S., Tang, L., Zhang, W., Lu, X., 2010. A detailed pollen record of vegetation and climate changes in Central China during the past 16,000 years. Boreas 39, 69–76.
Zhu, G., Wang, C., Liu, Z., Ohtani, S., 2013. Studies on species composition of phytoplankton in Fuxian Lake of Yunnan, China. Adv. Mater. Res. 807–809, 1695–1701.
Zhu, G., Qin, D., Liu, Y., Chen, F., Hu, P., Chen, D., Wang, K., 2017. Accuracy of TRMM precipitation data in the southwest monsoon region of China. Theor. Appl. Climatol. 129, 353–362.